Analysis and Emulation of Actuating Forces on Wind Turbine Pitch Drives

Facundo Enrique Gonzalez

Victor Juliano De Negri

Federal University of Santa Catarina
Department of Mechanical Engineering – LASHIP Laboratory of Hydraulic and Pneumatic Systems, Campus Universitário - ZIP Code:88040-900 – Florianópolis - SC - Brazil -Phone (+55) 48 3721 7714 – E-Mail: fakgonzalez@gmail.com; victor@emc.ufsc.br

João Marcos Castro Soares

Reivax Automation and Control
Rod. José Carlos Daux - Km1 – Tecnópolis – Florianópolis –SC –Brazil – Phone: (+55) 48 3027-3700. E-Mail: jms@reivax.com.br

Abstract

This paper presents the study and modeling of the actuating forces at pitch control systems of wind turbines as well as the development of a loading emulation system as part of a test rig for experimental evaluation of pitch control systems. The force modeling presented is based on the wind blade geometry, which is one of the parameters of greatest influence in the actuating force magnitude. Consequently, the Blade Element Momentum theory (BEM) and the equations that model friction, gravitational, inertial, and wind resulting dynamic forces are took into account. The hardware in the loop simulation technique (HIL) is being applied where the actuating force is calculated by a real-time software considering several parameters such as wind speed, blade geometry, pitch angle, etc. A hydraulic force control system consisting of a hydraulic cylinder controlled by two high response proportional pressure reducing valves tracking the force reference signal is presented. This test rig emulates forces in agreement to turbines up to 700 kW but the study presented in this paper can be used for the design of pitch drivers in general.

KEYWORDS: pitch drive, wind turbine, actuating forces, hydraulic systems

1. Introduction

A growing development has been observed in all areas related to the design and construction of wind turbines where the optimization of the conversion of wind resource into electric energy has became an important issue. This aspect is particularly

considerable for higher power units where an efficiency increase can result in a substantial quantity of delivered energy.

In this scenery, the development of pitch drive systems and pitch control strategies has being carried out in the last years. In the control of horizontal axis wind turbines, the pitch angle variation makes possible to optimize the energy capture, to reduce the dynamic loads at the turbine structure, and to maintain the quality of the generated power according to the standard requirements.

The pitch drive (PD) has the important function of limiting the mechanic power transmitted to the electric generator for those situations in which the available wind speed exceeds the nominal speed. In **Figure 1** the typical operational strategy of a wind turbine can be seen, in which the turbine starts operating at point A and from there until point B the operational strategy consists in optimizing the power coefficient (C_P) running with variable rotor angular speed. From point B to C the rotor angular speed is kept in its nominal value and from point C the delivered power is limited changing the pitch angle. At point D, where the cut-off wind speed is reached, the equipment is taken out of operation for safety reasons.

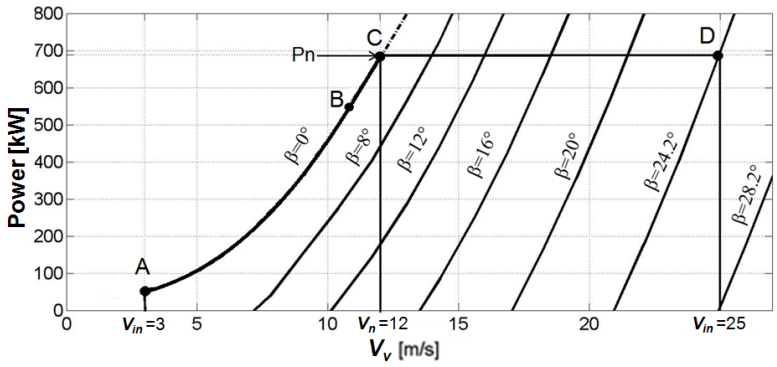

Figure 1: Characteristic power curve of a 700 kW wind turbine

One of the main requirements of a PD system is the total force that the actuators must support. Bosssanyi & Jamieson /1/ study the influence of significant factors like the bearing friction and the torsional stiffness of the blade. In Yao *et al.* /2/ it is presented the determination of forces with emphasis in the moment due to the distribution of the mass in the blade profile, minimizing the influence of aerodynamic moment and the bearings friction moment. In Dai *et al.* /3/ and Caselitz *et al.* /4/ different forces that act over a turbine blade are obtained, departing from a Blade Element Momentum (BEM) algorithm modified with the dynamic stall model.

However, these studies do not include experimental results. Experimental studies for turbine subsystems like the PD have some characteristics that make their implementation difficult, such as the huge masses to be moved, the high force values, and the high dynamics of those forces depending on variable and uncontrollable sources like the wind speed.

Among the studies including PD experiments, Caselitz *et al.* /5/ analyze the dynamic behavior of an electromechanical PD using a hardware in the loop (HIL) strategy. Chiang *et al.* /6/ present a system also using a HIL analysis where a hydraulic system controlled by the rotational frequency of the pump is used. In this study the perturbation of the system is made by hydraulic cylinders that reproduce the effect due to the tower shadow. In Wu *et al.* /7/ a force emulation system is applied to evaluate adaptive estimation-based leakage detection. The experimental system has a work scale of 1000:1 both in force values as well as in their dimensions.

In the study here presented, firstly, all the forces acting on the PD are presented, secondly, the experimental system that works with the HIL technique applied to an individual hydraulic acting system is presented, and finally, preliminary experimental results of the system of emulation of forces are shown.

2. Actuating forces on pitch drive mechanisms

A hydraulic PD mechanism acting individually on a wind turbine blade (WTB) is presented in **Figure 2.** In this figure, the possibility of variation of pitch angle through the displacement of the piston rod from point A to point B is observed. The control cylinder has to generate the hydraulic force (F_p) which produces a moment that needs to compensate the load moment (T_L), such that, considering it as a rigid system, the blade movement can be expressed according to the Newton´s second law by

$$F_P r_p \cos(\beta) + T_L = I_B \ddot{\beta} \tag{1}$$

The load moment (T_L) is the result of several issues that need to be carefully analyzed for the design of PD control systems. In this study, blade geometric parameters like the variation of the chord and the twist for each section, the aerodynamic profile, the longitudinal axis position and its mass distribution are considered. The different forces that contribute to the load moment are presented in the following sections.

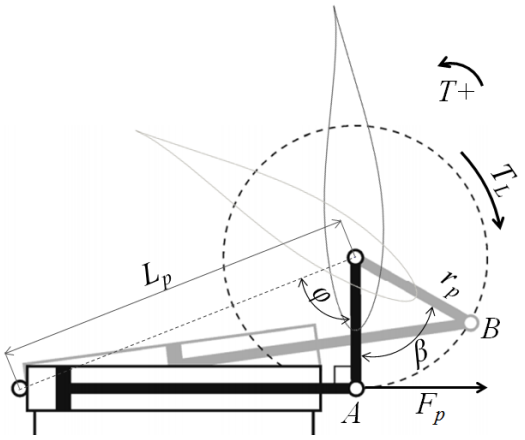

Figure 2: Hydraulic pitch drive mechanism (adapted from /8/)

2.1. Aerodynamic moment

The aerodynamic forces that act on a blade section are presented in **Figure 3**. The point Z indicates the intersection of the blade rotation longitudinal axis with the section plane, point A represents the leading edge, and point C is the centre of pressure where the aerodynamic force caused by the dynamic pressure can be represented like a punctual force.

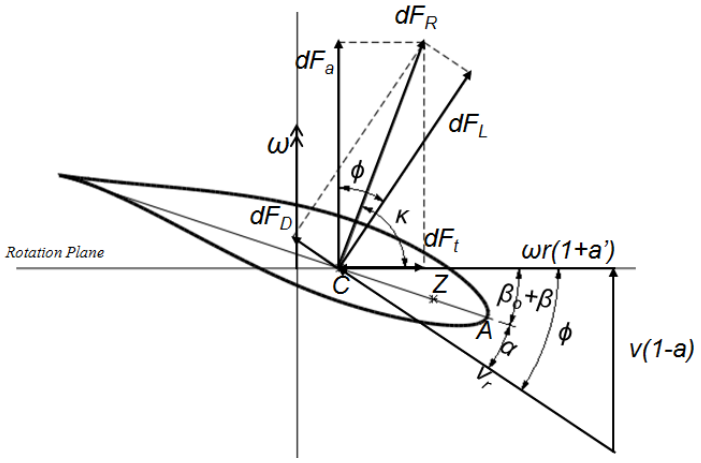

Figure 3: Aerodynamic forces on a Blade Element /5/

The factors *a* and *a'* (Figure 3) need to be found in an iterative way in the BEM algorithm. In this study the algorithm presented in /5/ is used considering the incidence of the wind always perpendicular to the swept area. Such that the aerodynamic resulting force is

$$dF_R = \frac{1}{2}\rho v_r^2 c\sqrt{C_L^2 + C_D^2}\,dr \tag{2}$$

The angle between the resulting force (dF_R) and rotation plane can be expressed by

$$\kappa = \arctan\frac{dF_a}{dF_t} = \arctan\ \frac{C_L\cos(\varphi)+C_D\sin(\varphi)}{C_L\sin(\varphi)\ \ C_D\cos(\varphi)} \tag{3}$$

The moment resulting from the dF_R using as a reference the leading edge (point A) can then be expressed as

$$dT^A_{aero} = dF_R\sin(\beta+\beta_o+\kappa)AC \tag{4}$$

This moment can also be expressed as a function of the moment coefficient (C_m) /5/ such that

$$dT^A_{aero} = \frac{1}{2}\rho C_m v_r^2 c^2 dr \tag{5}$$

Considering that the location of the longitudinal rotation axis (Point Z) is defined at the blade design, the distance between this point and the centre of pressure (C) is determined from the combination of equations 2, 4, and 5 such that

$$ZC = AC - AZ = \frac{C_m c}{\sqrt{C_L^2+C_D^2}\sin(\beta+\beta_o+\kappa)} - AZ \tag{6}$$

The aerodynamic moment in a section of the blade, caused by dF_R, from a distance ZC of the rotation axis C can be expressed similarly to Equation 4 as

$$dT^Z_{aero} = \frac{1}{2}\rho v_r^2 c\sqrt{C_L^2+C_D^2}.\sin(\beta+\beta_o+\kappa)ZC.dr \tag{7}$$

Finally, aiming at evaluating the total aerodynamic moment throughout the whole blade, the following equation can be applied:

$$T^Z_{aero} = \frac{1}{2}\rho\int_{Ro}^{R} v_r^2 c\sqrt{C_L^2+C_D^2}.\sin(\beta+\beta_o+\kappa)ZC.dr \tag{8}$$

2.2. Bearing friction moment

The resulting friction moment depends on the static and dynamic frictions /9/. The static friction is directly related to the load to which the bearing is submitted. Various models depending on the speed can be found in the literature for the dynamic friction. However, in the PD the acting speeds are relatively low due to the limitations caused by the structure of the blade. For special situations such as emergency stops, the speed can reach maximum values in which the effect of the static loads still continues to be dominant. Therefore, the moment due to the friction in the bearings can be calculated by

$$T_f = \frac{\mu_r}{2}\left(4.4M_k + F_{aR}D_{mR} + 2.2F_{rR}D_{mR}1.73\right) \quad (9)$$

which is obtained empirically /10/. The friction coefficient (μ_r) is determined by the bearing type, the total moment (M_k) is the resultant of all the moment acting in the bearing plane direction. F_{aR} is the resultant of all axial forces, including the centrifugal force of the blade, and F_{tR} is the resultant of all tangential forces acting on the blade. The mean diameter (D_{mR}) of the bearing is taken from the manufacturer catalogue.

2.3. Gravity moment

Assuming that the blade gravity centre is displaced at a distance (r_{cg}) from the longitudinal axis of blade rotation, the corresponding moment on the PD is expressed by

$$T_{gi} = mgr_{cg}sin(\beta + \beta_o + \theta)cos(\omega t) \quad (10)$$

Where (m) is total mass of blade, (g) is gravity constant and (t) is the time.In the case of a collective single actuator, this moment is not taken into account because it is canceled due to the symmetric distribution of the moments in the 3 blades acting in only one mechanism /1/.

2.4. Centrifugal inertial moment

The mass distribution in each section of the blade causes the different centrifugal acting forces in each point to generate a moment on the PD like it is shown in **Figure 4**. This moment can reach significant values and according to Stoddard *et al.* /11/ its value is determined by

$$T_{CI} = \frac{1}{2}\omega^2 \int_{R_o}^{R} \rho_{blade}\left(I^S_{max} - I^S_{min}\right)sin\left(2(\beta + \beta_o)\right)dr \quad (11)$$

2.5. Total load moment

Based on the moments previously presented, it is possible to determine the load moment as

$$T_L = T^Z_{aero} - T_f + T_{gi} + T_{CI} \quad (12)$$

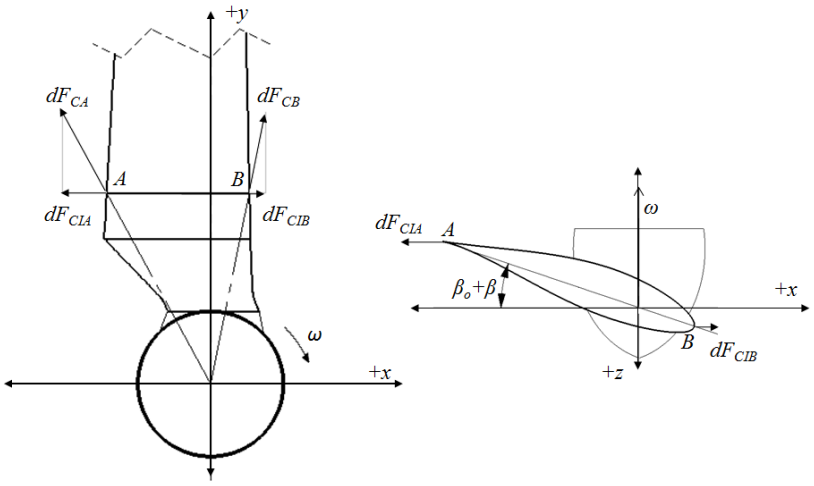

Figure 4: Centrifugal inertial moment

3. Experimental test rig

From the load moment (T_L) it is possible to find the force reference that will be emulated at the test circuit shown in **Figure 5.** This test rig consists of a pitch cylinder (Bosch Rexroth CDT3MT4/80/56/500/Z/1X/B11 HFDTWW) which is controlled by a proportional directional valve (PDV) (ATOS DHZO-TE-071-L5/1 40) and its feedback position is measured by an incremental encoder (Veeder Root B58N). Furthermore, a loading cylinder generates an opposing force which depends on different conditions such as the wind speed, the angular speed, and the pitch angle, according to the equations presented in Section 2. This cylinder is equal to the pitch cylinder being the force control achieved by controlling the chamber pressures independently by means of two closed loop controls using high response proportional pressure reducing valves (PRV) (Bosch Rexroth DREBE6X-1X/175MG24K31A1M) and pressure transmitters (HBM P2VA1/200bar).

The pressures in the chambers A and B are conjugated according to

$$T_L = A_A\left(\frac{p_B}{r_A} - p_A\right).r_L.cos(\beta) \tag{13}$$

where r_L is the moment arm of the load cylinder. In this case, r_L has the same value as r_p. The sign of the forces has such a convention that it is considered negative in the case that it generates a moment in the nose-down direction and positive in the nose-up direction of the airfoil /12/.

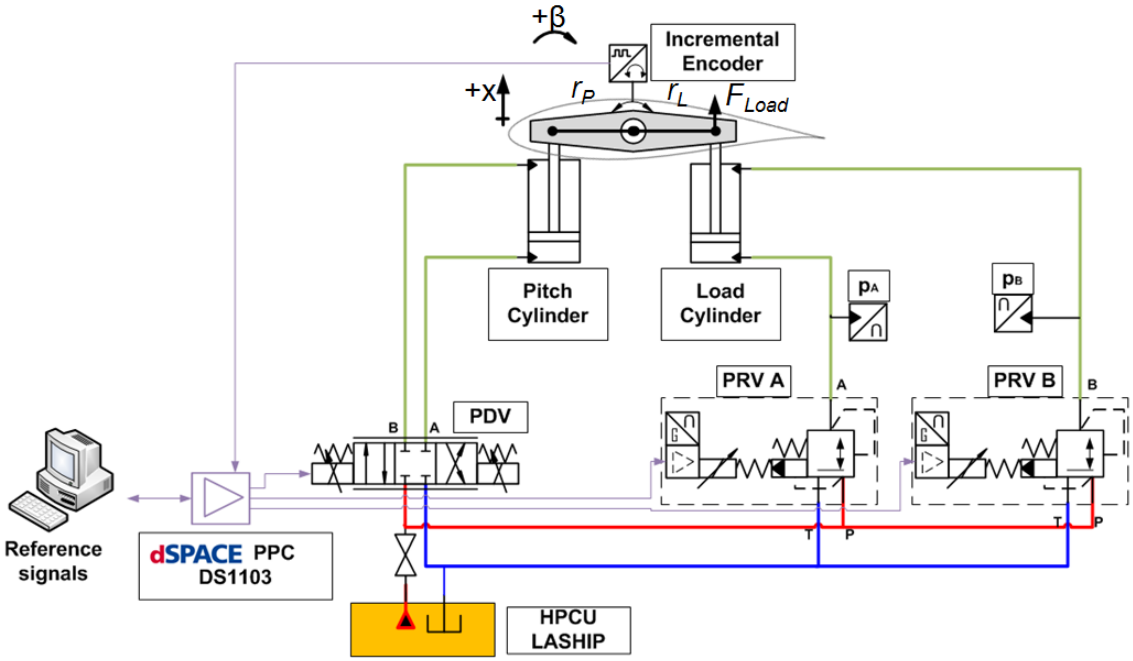

Figure 5: Test rig circuit

The experiments were carried out on a test rig as shown in **Figure 6.** A dSPACE® system was used for data acquisition and control working together with the Simulink/Matlab® and ControlDesk® software. For both simulations and experiments, an integration step of $1x10^{-3}$ s was used.

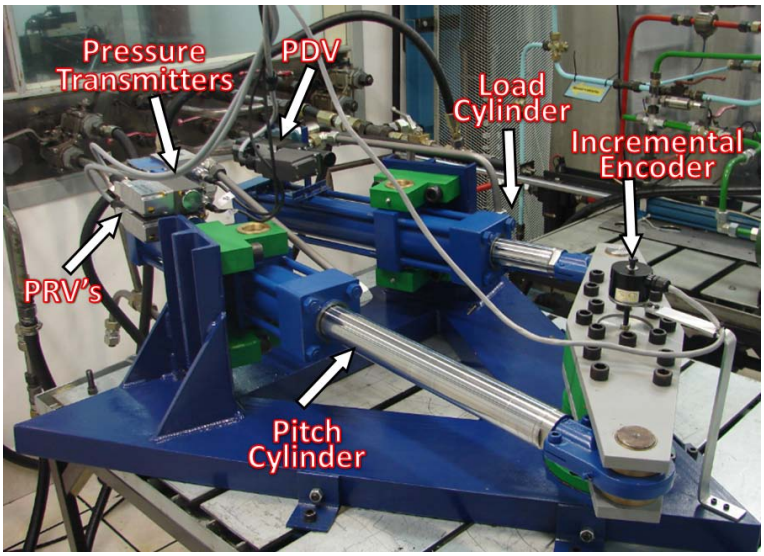

Figure 6: Test rig

For the positioning control a P controller was used with gain equal to 3. For the pressure control a PID controller was used for each chamber. For the pressure control in chamber A, the chosen gains where P=0.01, I=0.06, and D=0.01 and for chamber B, P=0.02, I=0.1, and D=0.015. The supply pressure was 10 MPa.

4. Experimental results

Figure 7 presents some results regarding to the system response for pitch angle step inputs between 0° and 8° and a constant load force reference kept at -10000 N. Steady state position errors of 0.043º for the 0º position and of -0.088º for the 8º position and a settling time of 1.15 s in both cases were obtained. In spite of the positioning system to be using just a proportional controller the rise time is quite similar to that obtained by Miller et al. /13/. The force error achieved a mean value of 121 N in steady state and a maximum steady state error of 177.7 N.

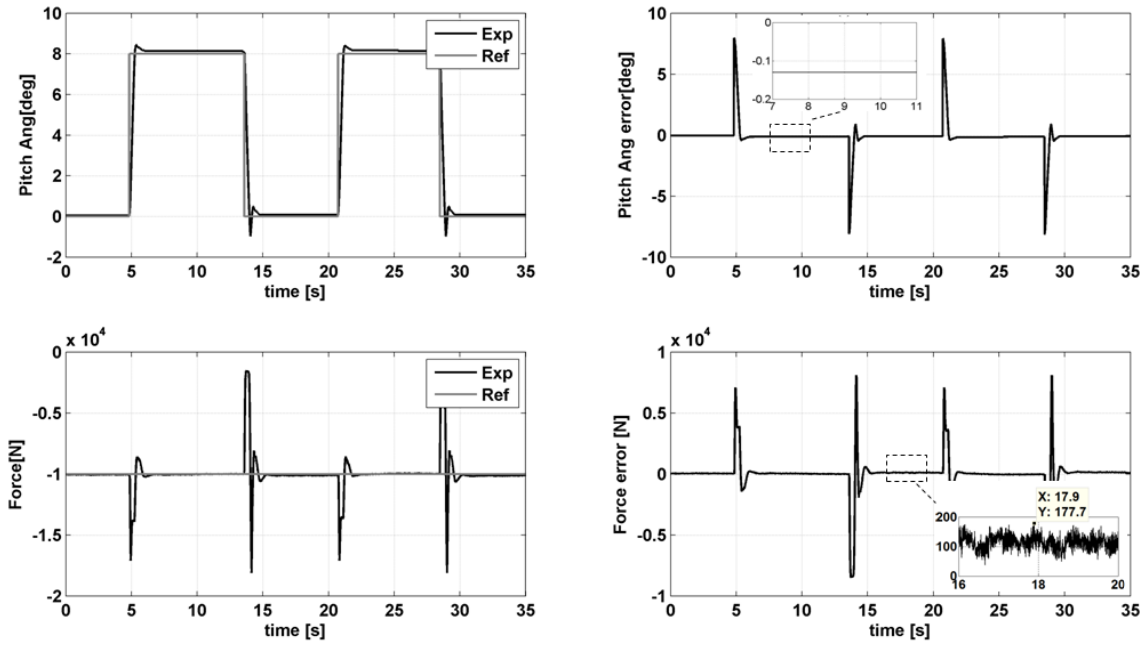

Figure 7: Position step experimental responses

As it was presented in Section 2, the effective forces at wind turbines are variable depending on several factors. One of these factors is the pitch angle such that the reference force will not be constant when an angle changing occurs.

A force step response analysis was carried out to evaluate the force emulation system as shown in **Figure 8**. Steps between -10000 to -5000 N were applied perturbing the positioning system. The mean steady state error was -135 N with a settling time of 0.75 s. from where one can estimate a loading system natural frequency around 13 rad/s (2 Hz). Otherwise, the maximum wind frequency, corresponding to the turbulence component, is around 1.57 rad/s (0.25 Hz) /14/ such that the designed force emulation system will be able to reproduce dynamically the desired forces.

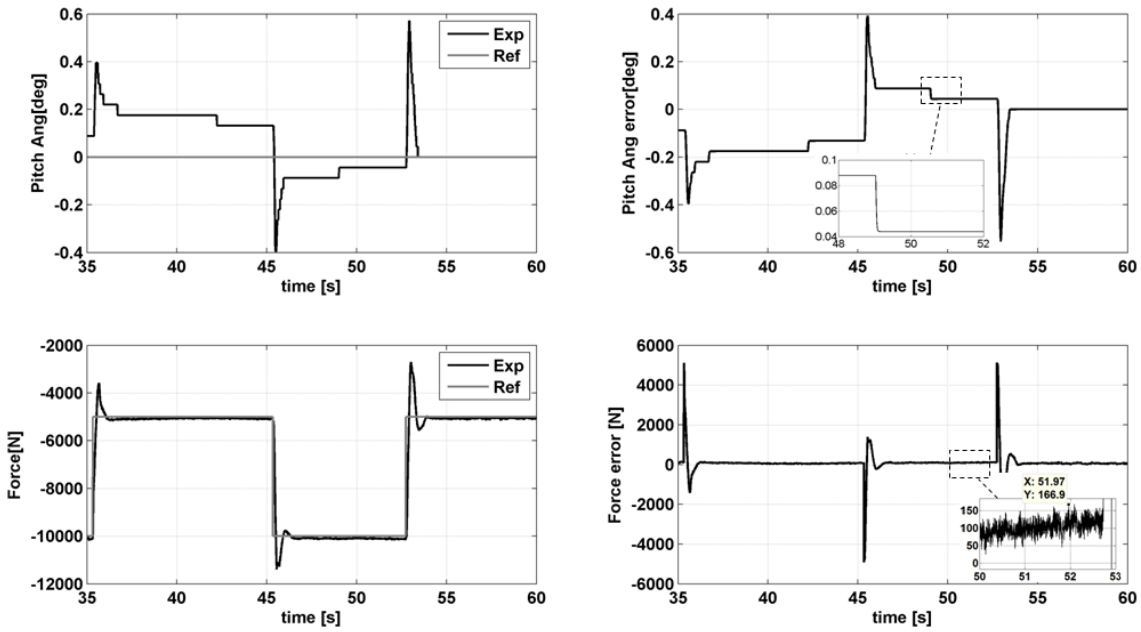

Figure 8: Force step response

5. Conclusions

In this paper the equations of the acting forces of a hydraulic individual PD are presented. The acting forces are dependent of factors such as blade geometry, wind speed, angular rotor speed, and blade pitch angle. These forces are also used as an input of a force emulation system which is implemented by means of a HIL structure. The force control is carried out by independent pressure control in the load cylinder chambers using proportional pressure reducing valves. Preliminary experimental results demonstrate the emulation system capability to generate load forces for the pitch angle control system development.

6. Acknowledgments

This research is being support by the Foundation for Support of Research and Innovation of the State of Santa Catarina (FAPESC) and REIVAX Automation and Control.

7. References

/1/ BOSSANYI, E. A., JAMIESON, P., *Blade pitch system modelling for wind turbines,* European Wind Energy Conference 1999, Nice, France, pp. 893-896.

/2/ YAO, X., SHAN, G., SU, D., *Study on variable pitch system characteristics of big wind turbine,* International Technology and Innovation Conference 2006, Hangzhou, China, pp. 2239-2243.

/3/ DAI, J. C., HU, Y. P., LIU, D. S., LONG, X., *Calculation and characteristics analysis of blade pitch loads of large scale wind turbines.* Science China Technological Sciences 2010, 53: pp. 1356-63.

/4/ DAI, J. C., HU, Y. P., LIU, D. S., LONG, X., Aerodynamic loads calculation and analysis for large scale wind turbine based on combining BEM modified theory with dynamic stall model. Renewable Energy 36, 2011. Pp. 1095-1104.

/5/ CASELITZ, P., GEYLER, M., GIEBHARD, J., PANAHANDEH, B., *Hardware in the loop development and testing of new pitch control algorithms.* European Wind Energy Conference 2006, pp. 60-64, Athens, Greece, 2006.

/6/ CHIANG, M. H., CHEN, Y. N., LIN, H. T., CHANG, Y. Y., *A variable-speed pump-controlled hydraulic servo system for a novel pitch control system of wind turbines.* 7th International Fluid Power Conference 2010, Aachen, Germany

/7/ WU, X., LI, Y., LI, F., YANG, Z., TENG, W., *Adaptative estimation-based leakage detection for a wind turbine hydraulic pitching system.* IEEE Transactions on mechatronics 2011. V. PP: 99, pp. 1-8.

/8/ HANSEN, M. N., *How hard can it be to pitch a wind turbine blade?*. RISO Lab, Denmark Tech. Univ. Kongens Lyngby, Denmark, 2007.

/9/ LEKOU, D. J., MOUZAKIS, F., SAVENIJE, F. J., *Procedures for testing and measuring wind energy systems.* Centre for renewable energy sources and saving, 2010, Pikermi, Greece.

/10/ ROTHE ERDE, *Slewing Bearings.* Dortumdn, Germany, 2011, available at http://www.rotheerde.com/download/info/Rothe_Erde_GWL_GB.pdf.

/11/ STODDARD, F., NELSON, V., STARCHER, K., ANDREWS, B., *Determination of elastic twist in horizontal axis wind turbines,* National Renewable Energy Laboratory, 1989, Canyon, Texas, 170 p.

/12/ BURTON, T., SHARPE, D., JENKINS, N., BOSSANYI, E., *Wind Energy Handbook* Chichester, England, Jhon Wiley, 2001; 643 p.

/13/ MILLER, N. W., SANCHEZ-GASCA, J. J., PRICE, W. W., DELMERICO, R. W., *Dynamic modeling of GE 1.5 and 3.6 MW wind turbine-generators for stability simulations.* Power Engineering Society General Meeting, 2003,

IEEE, pp.1977-1983.

/14/ NICHITA, C., LUCA, D., DAKYO, B., CEANGA, E., *Large band simulation of the wind speed of real time wind turbine simulators.* IEEE Trans. On Energy conversion, [S.1.],V.17, n. 4, Dec. 2002.

8. Nomenclature

a,a'	axial, tangential factor	-	r_{cg}	distance gravity center - pitch axis	m
A_A	area A of cylinder	m^2	R_o,R	initial/final length blade	m
c	chord length	m	r_p	blade-arm mechanism radio	m
$C_{L,D,m}$	lift, drag, moment coeff.	-	T_{Cl}	centrifugal moment	Nm
D_{mR}	bearing mean diameter	m	T_f	friction moment	Nm
F_a,F_t	axial, tangential forces	N	T_{gi}	gravity moment	Nm
$F_{aR,rR}$	bearing axial, radial force	N	T_L	load moment	Nm
$F_{C\,A,B}$	centrifugal force in A, B	N	T^z_{aero}	aerodynamic moment	Nm
F_L,F_D	lift, drag force	N	v_r	relative wind speed	m/s
F_p	hydraulic force	N	α	angle of attack	rad
I_B	blade polar inertia	kgm^2	β	pitch angle	rad
$I^S_{max,}$ I^S_{min}	max, min 2nd moment of inertia on the section	m^4	β_o	twist angle	rad
L_p	fixed point distance	m	μ_r	friction coefficient	-
M_k	bearing total moment	Nm	ρ	air density	kg/m^3
$p_{A,B}$	pressure in chamber A, B	Pa	ρ_{blade}	blade density	kg/m^3
r	local element radius	m	φ	mechanical initial angle	rad
r_A	area ratio	-	ω	rotor angular speed	1/s